Biophysical Journal
Article

Biophysical Society

Hidden intermediates in Mango III RNA aptamer folding revealed by pressure perturbation

Balasubramanian Harish,[1,5] Jinqiu Wang,[1] Eric J. Hayden,[2] Bastian Grabe,[4] Wolf Hiller,[4] Roland Winter,[3] and Catherine A. Royer[1,*]

[1]Department of Biological Sciences, Rensselaer Polytechnic Institute, Troy; [2]Department of Biology, Boise State University, Boise; [3]Physical Chemistry I - Biophysical Chemistry, Department of Chemistry and Chemical Biology, TU Dortmund University, Dortmund, Germany; and [4]Department of Chemistry and Chemical Biology, TU Dortmund University, Dortmund, Germany

ABSTRACT Fluorescent RNA aptamers have the potential to enable routine quantitation and localization of RNA molecules and serve as models for understanding biologically active aptamers. In recent years, several fluorescent aptamers have been selected and modified to improve their properties, revealing that small changes to the RNA or the ligands can modify significantly their fluorescent properties. Although structural biology approaches have revealed the bound, ground state of several fluorescent aptamers, characterization of low-abundance, excited states in these systems is crucial to understanding their folding pathways. Here we use pressure as an alternative variable to probe the suboptimal states of the Mango III aptamer with both fluorescence and NMR spectroscopy approaches. At moderate KCl concentrations, increasing pressure disrupted the G-quadruplex structure of the Mango III RNA and led to an intermediate with lower fluorescence. These observations indicate the existence of suboptimal RNA structural states that still bind the TO1-biotin fluorophore and moderately enhance fluorescence. At higher KCl concentration as well, the intermediate fluorescence state was populated at high pressure, but the G-quadruplex remained stable at high pressure, supporting the notion of parallel folding and/or binding pathways. These results demonstrate the usefulness of pressure for characterizing RNA folding intermediates.

SIGNIFICANCE G-quadruplex RNA structural dynamics are important for pre-mRNA maturation, mRNA transport, stability, and translation, genome duplication and maintenance via telomerase RNA transitions. Understanding the sequence-structure relationships and folding pathways for these RNA structures remains challenging. High hydrostatic pressure represents an alternative perturbation to high temperature or low ionic strength that allows for enhanced population of RNA structural excited states. High hydrostatic pressure was coupled to fluorescence and 1D ^{1}H NMR to reveal and characterize intermediates in the folding pathway of the fluorescent RNA Mango III aptamer.

INTRODUCTION

RNA molecules perform numerous important biological functions (1–5) but can be challenging to study because they are dynamic in space and time (6,7). In recent years advances in single-molecule fluorescence resonance energy transfer (e.g., Bisaria and Herschlag (8)) and multidimensional NMR (e.g., Bothe et al. (9)) have provided insights into RNA conformational heterogeneity and excited state structure and dynamics (10–13). In particular, fluorescent labeling of specific RNA molecules is critical for studying the biological roles of both coding and noncoding RNA. Fluorescent RNA aptamers are RNA molecules selected to bind and significantly enhance the fluorescence of their ligands. Because these RNA aptamers are relatively small and can be genetically encoded, they have proven useful for the quantitation and localization of RNA molecules in living cells, much the way fluorescent protein fusions have enabled protein research. Despite recent advances from several research groups, improvements are still needed in aptamer properties such as brightness, stability, and affinity. However, the sequence to function relationships for these systems remain poorly understood, impeding the improvement of their properties by either rational design or selection. Contributing to this challenge is the fact that several fluorescent aptamers have a G-quadruplex binding site (14–16). Prior investigations have suggested that RNA

Submitted June 6, 2021, and accepted for publication December 23, 2021.

*Correspondence: royerc@rpi.edu

Physical Chemistry I - Biophysical Chemistry, Department of Chemistry and Chemical Biology, TU Dortmund University, Dortmund, Germany

Editor: Susan Schroeder.

https://doi.org/10.1016/j.bpj.2021.12.037

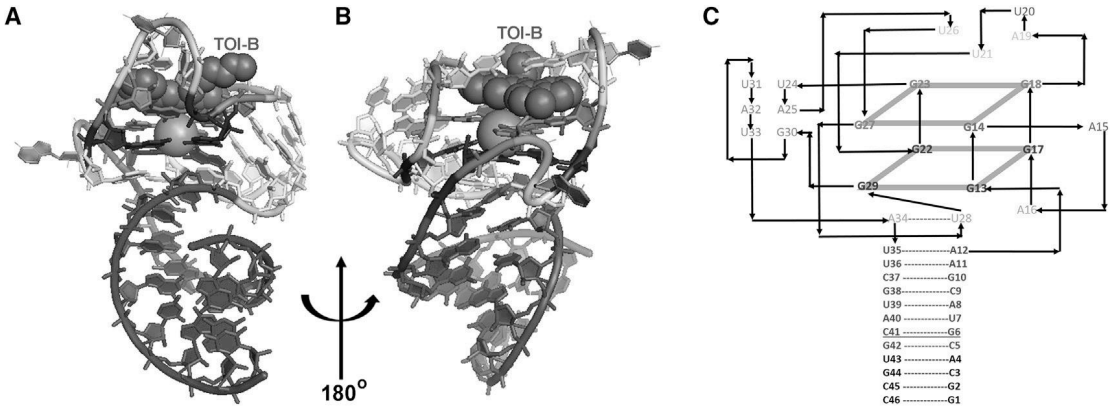

FIGURE 1 Structure of the Mango III aptamer. (*A* and *B*) Two 180° orientations of the original Mango III aptamer structure (PDB: 6e8s) reported in Trachman et al. (15). Lower (dark blue) and upper (teal) G-quadruplexes are capped by dye (TOI-B, purple spheres). The dye is capped by the canonical WC A-U basepair (yellow). The G-quadruplex is stabilized by a potassium ion (large green sphere) and interacts with a flanking helix of WC basepairs (wheat). Underlying the G-quadruplex are three hydrogen-bonded bases A30-U24-A12 (light pink) followed by a canonical double helix (red). Two bases, A11 and U16 (CPK colors), are extruded from the structure, and one base, U21 (pale green), interacts with the dye. (*C*) Topology of the Mango aptamer structure used in the present study (color coded as in *A* and *B*), which has four extra basepairs in the bottom stem (in black), and the basepair, G6-C41 (underlined in red), in that stem is inversed compared with the crystal structure in which it is the second basepair, C2-G37.

G-quadruplex structures are dynamic in biological systems, and that their folding and unfolding is functionally relevant. For example, G-quadruplex RNA structural dynamics are important for pre-mRNA maturation, mRNA transport, stability, and translation, genome duplication and maintenance via telomerase RNA transitions (17,18). It is possible that G-quadruplex structural dynamics might play important roles in fluorescent RNA aptamers as well, but the dynamics of these structures are not well studied.

RNA aptamer-ligand interactions are often modeled as a two-state system. However, there are numerous RNA structural intermediates that might contribute to ligand binding in various ways. The ability to study RNA conformations depends on the degree to which excited state conformations are populated. NMR relaxation approaches have allowed mapping of excited state structures of biomolecules (19,20) but remain limited to those that are well populated under standard conditions. The effect of pressure on RNA structures provides a means to favor excited states so they can be studied. Pressure perturbation has been shown to favor the population of partially disrupted, excited states of proteins. These states are characterized by a decrease in the number of stabilizing interactions relative to the ground state and are consistent with more dynamic structures that can allow for more efficient ligand binding (21–23). These structures are populated under high pressure conditions because they exhibit smaller molar volumes than fully folded states.

Although pressure in general does not significantly destabilize canonical nucleic acid double helices (24–27), it can have significant effects on more complex nucleic acid structures. For example, pressure has been shown to disrupt DNA G-quadruplex structures (28–33), with volume changes for transitions to "unfolded" or disrupted states of $\sim$ –30 to −60 mL/mol, on the order of those observed for protein unfolding. Ribonucleic acid hairpins or tetraloops can be either slightly stabilized or slightly destabilized by pressure, depending upon the sequence of the loop (34–36). Ribozyme function is generally inhibited by hydrostatic pressure, due to positive activation volumes for the reactions (37–40), and subtle effects of pressure on tRNA structure based on high-pressure Fourier transform infrared spectroscopy studies have been reported (41). However, molecular insight into the actual structural changes in RNA molecules caused by pressure perturbation remains extremely limited. In addition to its utility in mapping conformational landscapes of biomolecules, understanding pressure effects on biomolecules is essential in that much of the microbial biomass on Earth is found in the deep biosphere, where pressures can reach hundreds to thousands of atmospheres (42–48). Moreover, life is thought to have originated with RNA-based chemistry (49), possibly at hydrothermal vents in the deep ocean where it would have been protected from bombarding radiation on the early Earth.

To evaluate structurally dynamic states of fluorescent RNA aptamers, we characterized pressure effects on the Mango III aptamer (15,16). Several structural variants of the Mango aptamer have been selected with the goal of improving single-molecule RNA detection in vivo (15,50,51). They bind a visible fluorescent dye, thiazole orange-biotin (TO1-B, labeled TO here) that is strongly quenched in water or in presence of nonspecific RNA, but which undergoes a >1000-fold increase in fluorescence intensity when bound to its target RNA (50). The Mango III RNA aptamer forms a two-layered G-quadruplex structure, seated on a canonical double helix and flanked by a second helical element (Fig. 1) (15). The Mango III sequence used in this study (GGCACGUACGAA GGAAGGAUUGGUAUGUGGUAUAUUCGUACGUGCC) differs slightly from that in the structure in Fig. 1 only in the length and sequence of the double-stranded helical segment underpinning the G-quadruplex structure. The TO dye intercalates between the upper G-quadruplex and a canonical A-U

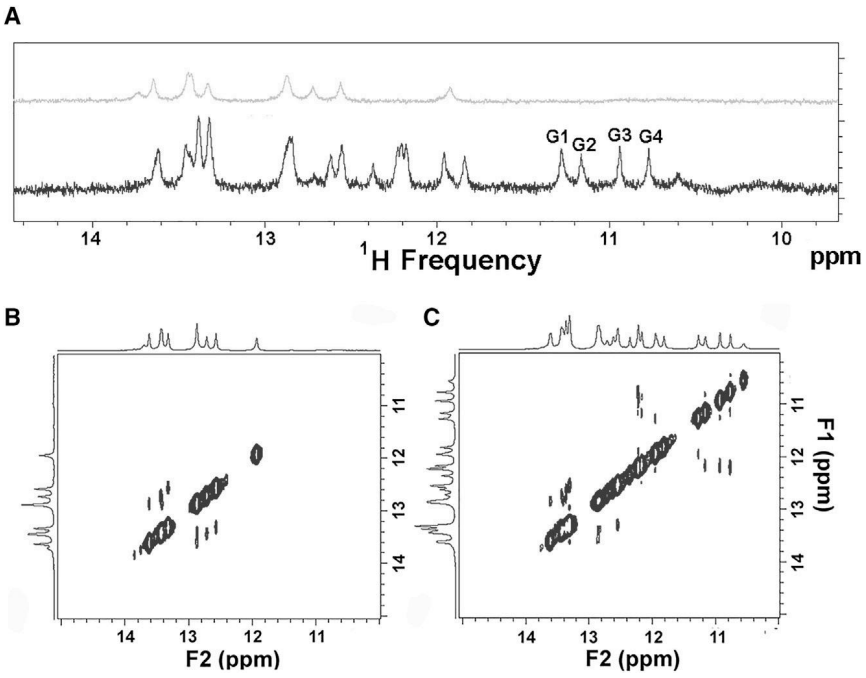

FIGURE 2 ^{1}H NMR spectrum of Mango III at 10 mM KCl. (*A*) 1D ^{1}H NMR spectra in absence of dye (yellow) and in presence of TO (blue). The most prominent peaks to appear in the G-quadruplex imino range are labeled G1–G4. (*B*) 2D ^{1}H–^{1}H NOE spectra in absence of dye and (*C*) in presence of dye. Spectra were acquired in 20 mM MOPS buffer, 20°C (pH 7.2). Several new peaks appear in the 1D spectrum, both in the G-quadruplex region (∼11–12 ppm) and in the duplex region (∼12–14 ppm) upon addition of TO and correspond to imino protons that become protected upon stabilization of the G-quadruplex by the dye. Three NOEs between G-quadruplex imino protons and three NOEs between duplex imino protons and the G-quadruplex amino/aromatic protons also appear upon TO binding. NOESY spectra were acquired using a 700-MHz spectrometer equipped with a cryoprobe.

basepair (underscored in the above sequence) above it. Here we used fluorescence and NMR under conditions of variable ionic strength and high pressure to observe changes in structural states of Mango III. We found that pressure leads to the population of at least two intermediate states of Mango III. In one of these intermediates, populated at high pressure and intermediate salt concentration, the G-quadruplex structure is disrupted, yet the aptamer retains some interactions with the TO dye, leading to an intermediate fluorescence intensity, similar to that observed for Mango IV. At higher salt concentration, the high-pressure intermediate retains an intact G-quadruplex, but a reduced fluorescence level relative to the fully folded aptamer.

MATERIALS AND METHODS

Materials

Mango III RNA oligo (5′-GGCACGUACGAAGGAAGGAUUGGUAUGUGGUAUAUUCGUACGUGCC-3′) was purchased from Dharmacon (Lafayette, CO). TO1-PEG-Biotin dye was purchased from Applied Biological Materials (Richmond, BC, Canada).

High-pressure fluorescence

For fluorescence experiments, samples contained 2 μM RNA and 1 μM dye in 20 mM MOPS buffer at pH 7.2 and indicated KCl concentration. The setup for high-pressure fluorescence experiment has been previously described (52). The bound dye is excited at 495 nm, and fluorescence emission spectra were recorded from 520 to 570 nm. After pressurizing the sample, the sample was equilibrated for 60 min at each pressure before recording the final spectrum. Total intensity for each spectrum was calculated by integrating area under the curve.

High-pressure NMR

Samples for all NMR experiments contained 0.4 mM RNA and 0.4 mM dye in 20 mM MOPS buffer at pH 7.2 with 10% D2O and indicated KCl concentration. High-pressure 1D ^{1}H NMR spectra were acquired on a Bruker Avance III 600 MHz spectrometer in a standard 5-mm OD pressure-resistant zirconia tube from Daedelus Innovations. Hydrostatic pressure was applied to the sample using the Xtreme Syringe Pump (Daedelus Innovations, Aston, PA). Standard ^{1}H 1D experiments were performed with the zgesgp pulse sequence using excitation sculpting for solvent suppression. The sample was allowed to equilibrate for 60 min at each pressure before collecting data. At each pressure, 192 scans were collected with a recycle delay of 5 s. The spectra were processed and analyzed on Bruker's Topspin software.

2D nuclear Overhauser effect (NOE) data acquisition

Ambient pressure ^{1}H–^{1}H 2D NOESY experiments were performed on a Bruker Avance III 700 MHz spectrometer with a cryoprobe using the "noesyesgpph" pulse sequence with excitation sculpting for solvent suppression. The spectra were collected with 4096 points in the t2 dimension and 256 points in the t1 dimension, with a mixing time of 150 ms. 128 scans were collected with a recycle delay of 1 s. The data were processed and analyzed on Bruker's Topspin software.

High-pressure ^{1}H–^{1}H 2D NOESY experiments were performed on an Agilent DD2 500 MHz spectrometer using the "NOESY" pulse sequence with WET solvent suppression. The spectra were collected with 2048 points in the t2 dimension and 200 points in the t1 dimension, with a mixing time of 150 ms. At each pressure, 128 scans were collected with a recycle delay of 1 s. The data were processed and analyzed on VNMR and plotted on Mestrenova.

Data analysis

For both fluorescence and NMR experiments, intensity versus pressure curves were plotted and fitted to a two-state curve according to the equation

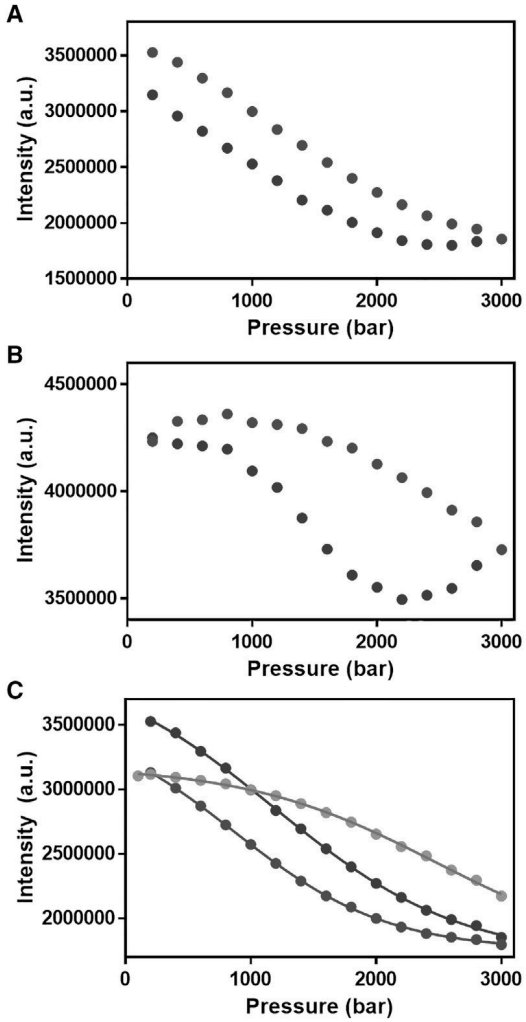

FIGURE 3 Pressure dependence of Mango III TO fluorescence. (*A*) at 10 mM KCl 20°C; (*B*) at 10 mM KCl 5°C (red: increasing pressure, blue: decreasing pressure); (*C*) Data and fits of the increasing pressure profiles at 1 (red), 10 (blue), and 100 (green) mM KCl and 20°C.

$$I = \left(I_{min} + I_{max} e^{(-(\Delta Go + p\Delta Vo)/RT)} \Big/ 1 + e^{(-(\Delta Go + p\Delta Vo)/RT)}\right) \quad \text{(Equation 1)}$$

where I is the intensity at a given pressure p, I_{min} and I_{max} are the plateau values at high and low pressures respectively, ΔV^o is the molar volume change, ΔG^0 is the free energy change at atmospheric pressure, R is the gas constant, and T is the temperature.

RESULTS

A stable Mango G-quadruplex structure is induced by ligand binding

The 1D proton and 2D proton NOE NMR spectra of the imino proton region of the Mango aptamer in absence of dye (Fig. 2 *A* and *B*) at 10 mM KCl exhibits peaks only in the chemical shift range known to correspond to canonical Watson-Crick basepairs. When dye is present at atmospheric pressure (Fig. 2 *A* and *C*), eight new peaks appear in the chemical shift range (10–12.4 ppm) known to correspond to imino protons engaged in Hoogsteen basepair interactions and thus protected from solvent exchange (53). These correspond to the imino protons of the eight guanosine bases implicated in the G-quadruplex structure (Fig. 1, teal and blue). The most prominent and upshifted peaks that appear in presence of dye are labeled G1–G4. Three NOE peaks of the four expected between the imino protons of the eight guanosine bases are observed in the 2D spectra, in addition to three of the four expected NOE peaks between the imino protons of the guanosines and those of bases in the underlying duplex. Finally, we observe several NOEs between the imino protons of the G-quadruplex and the aromatic-amino region of the spectrum (Fig. S1). Together these observations indicate that at 10 mM KCl at equilibrium at 20°C and near atmospheric pressure (10 bar), the Hoogsteen basepairs of the G-quadruplex of Mango III are unstable in absence of the TO dye.

Pressure leads to a partially fluorescent state of Mango III

The TO1-B dye is nearly completely quenched when free in solution or in presence of nonspecific RNA and exhibits a >1000-fold increase in intensity upon interaction with the Mango III RNA aptamer (15,50). The pressure dependence of the TO dye fluorescence of Mango III was monitored in 10 mM KCl, 20 mM MOPS buffer (pH 7.2) at both 5°C and 20°C (Fig. 3 *A* and *B*). At 20°C, the fluorescence intensity decreased by ~50%, nearing a plateau at 3 kbar. No change was observed below ~1500 bar at 5°C, and the total decrease was smaller than at the higher temperature, indicating a stabilization of the aptamer at low temperature. The observed ≤50% decrease at 20°C, reaching a high-pressure plateau, indicates the population of a distinct intermediate species by pressure in which the dye is exposed to solvent, but is not dissociated, since the fluorescence of the free dye is nearly 100% quenched. Rather, pressure induces a Mango III conformation in which the dye-RNA interactions have been altered. At both temperatures the return to atmospheric pressure revealed hysteresis that was more pronounced at 5°C, indicating that the system is not in true equilibrium. Fits of the profiles for increasing pressure yield apparent thermodynamic parameters (ΔG^o and ΔV^o) for the transition (Table 1). Profiles obtained at 1, 10, and 100 mM salt at 20°C are consistent with the known stabilization of the aptamer by potassium (Fig. 1). The similarity of the apparent volume change for the transition (ΔV^o) at all three salt concentrations indicates that the same transition is monitored. The value of $\Delta V^o = -32$ mL/mol is on the order of values (−22 to −68 mL/mol) previously reported for pressure disruption of DNA G-quadruplexes (30–32,54), although here the observable is dye fluorescence.

TABLE 1 Apparent thermodynamic parameters for the fluorescence-detected pressure-induced transition in Mango III at 20°C

[KCl] (mM)	ΔG^{o}_{app} (kcal/mol)	ΔV^{o}_{app} (mL/mol)
1	0.46 ± 0.03	−32.0 ± 1.6
10	0.93 ± 0.14	−32.7 ± 3.3
100	1.89 ± 0.16	−31.8 ± 5.6

The signs of ΔG^{o} and ΔV^{o} are for the "unfolding" direction of the reaction.

Pressure reversibly disrupts the Mango III G-quadruplex structure

We next examined the pressure effects on the fully folded dye-bound Mango III structure in 10 mM KCl using high-pressure proton NMR. Upon increasing pressure, the intensities of the imino proton resonances of the G-quadruplex decreased to nearly the level of the noise (Fig. 4) in a reversible manner (Fig. S2). The pressure dependence of the 2D NOE spectrum was also investigated (Fig. S3). The decreased sensitivity of the high pressure experiments (due to the necessity of using a 500-MHz spectrometer that is not equipped with a cryoprobe) resulted in the detection of fewer and weaker NOEs compared with the spectra in Fig. 2 (obtained using a 700-MHz spectrometer with cryoprobe). Nonetheless, the detected NOE peaks disappeared at 3000 bar. These observations indicate that pressure reversibly disrupts the G-quadruplex structure sufficiently to allow solvent exchange of these protons. Note that several other imino proton peaks are not significantly perturbed by pressure (Fig. 4). High-pressure 1D ^{1}H NMR experiments on Mango III were also carried out at 1 and 100 mM KCl (Figs. S4 and S5). In addition to peaks in the imino region of the spectrum, one resonance in the amino-aromatic region of the spectrum could also be quantified as a function of pressure (Figs. S6 and 5).

The pressure dependent loss of NMR peak intensity, at all three salt concentrations and 20°C, of the four most prominent G-quadruplex imino proton peaks between 10.8 and 12.4 ppm (Figs. 4, S3, and S4) were fit to a two-state model for the apparent ΔG^{o} and ΔV^{o} values of the transition (Figs. 5 and S7; Table 2). The stabilizing effect of KCl is apparent from the data and the fits. The curves for the imino protons obtained at 1 and 10 mM KCl appear to report on the same transition, stabilized at the higher salt. The values of ΔV^{o} for this transition at 1 and 10 mM KCl are similar (Table 2). They are also consistent with those observed for DNA G-quadruplex disruption under pressure (30–32,54). In contrast, the change in the intensities of the four G-quadruplex imino proton peaks and the amino/aromatic proton peak at 100 mM KCl were small and do not appear to report on the same pressure-induced transition as that which occurs at the lower salt concentrations.

DISCUSSION

We have reported structural states and fluorescence data of the Mango III aptamer under variable pressure, salt, and temperature conditions. Our results show that pressure can change the Mango III aptamer-ligand interaction by changing the dominant structural states of the RNA molecule. These results add to a growing understanding of how biomolecules respond to changes in pressure, and how pressure can be used as an experimental variable to investigate structure-function relationships.

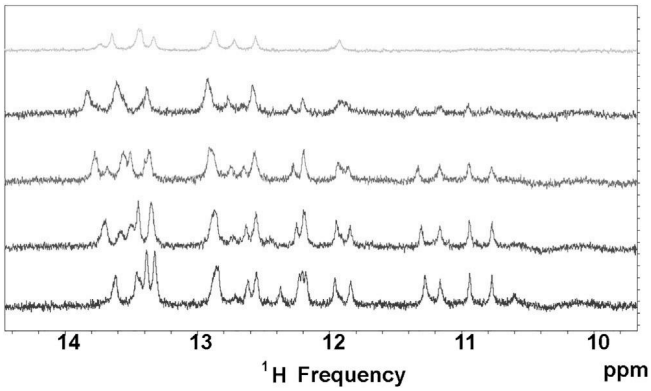

FIGURE 4 Pressure dependence of the imino region of the 1D ^{1}H NMR spectrum of Mango III. Pressures are 10 bar (blue), 1000 bar (red), 2000 bar (green), and 3000 bar (purple). The spectrum at atmospheric pressure in absence of dye is also shown for reference (yellow). All spectra were acquired in presence of TO except at atmospheric pressure, no dye (yellow). Experimental conditions were 10 mM KCl, 20 mM MOPS (pH 7.2), 20°C.

Induced fit by ligand binding to RNA

Our finding that at atmospheric pressure and 10 mM KCl, stable Mango III quadruplex formation is only observed in the presence of TO1-B is consistent with previous observations of RNA-ligand interactions. A compilation of binding kinetics showed that the association rates for small molecule RNA interactions are generally slower than diffusion, suggesting that many RNA molecules exist in different structural states when free or bound by ligand, and that binding and formation of the stabilized bound structure are coupled. Our results extend these observations to the unusual quadruplex structure of Mango III. Our data are consistent with an induced fit model because at 10 mM KCl, we see no evidence of the G-quadruplex structure at atmospheric pressure in the absence of TO1-biotin. However, our experiments cannot rule out that the G-quadruplex structure is sampled, but that the dynamic nature of the ensemble results in exchange of the G-quadruplex imino protons. Further experiments using isotope-labeled RNA would be needed to probe the structural dynamics of Mango III at atmospheric pressure to address the biophysical details of TO1-biotin binding (55).

Pressure leads to the population of intermediate states

Pressure effects on the Mango III structure arise from differences in molar volume between the various conformational

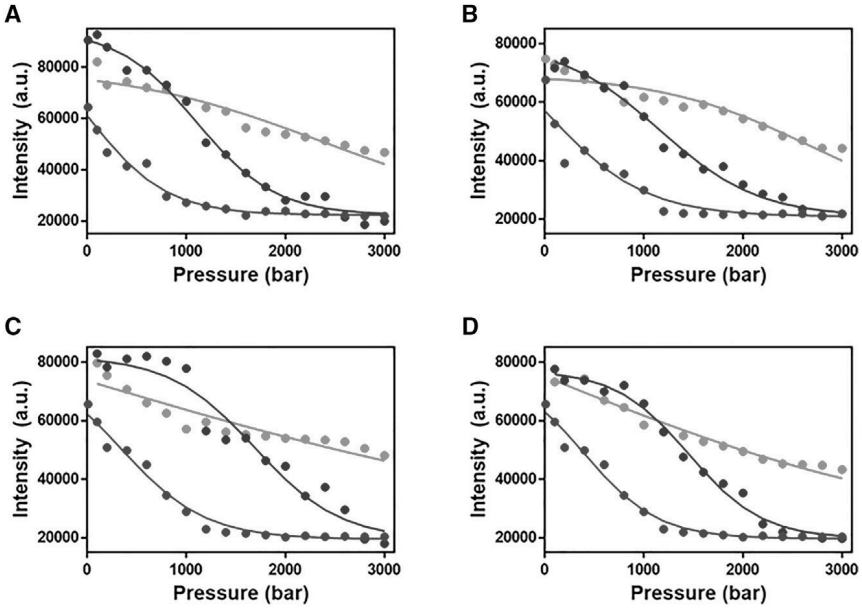

FIGURE 5 Pressure dependence of the intensity of the main G-quadruplex imino proton peaks in Fig. 2. (*A*) G1, (*B*) G2, (*C*) G3, and (*D*) G4. 1 mM KCl (red), 10 mM KCl (blue), and 100 mM KCl (green).

states of the aptamer. Negative volume changes for disruption of nucleic acid structure are essentially due to hydration of the exposed molecular surface and of the released ions upon unfolding (electrostrictive effect), ~6 mL/mol in the case of potassium ions (31). For particular cases, filling of void volume upon unfolding could play a role as well. Comparison of the high-pressure fluorescence and high-pressure NMR results at different KCl concentration reveals the pressure-induced population of at least two intermediate species in the folding of Mango III (Fig. 6).

Under all tested conditions, pressure leads to a modification of the interactions between the dye and the RNA, forming structural ensembles in which the dye is bound but ~50% less fluorescent. Free dye is 1000-fold less fluorescent than when bound to the Mango III RNA, and nonspecifically bound dye is seven-fold less fluorescent. Rather than the TO dye being unbound or nonspecifically bound, the ~two-fold decrease in fluorescence indicates a conformation that allows increased quenching by solvent, consistent with a decreased volume due to hydration. One scenario for the partial loss of fluorescence intensity is the unstacking of the TO dye molecule with the bases between which it intercalates, allowing entry of solvent and moderate quenching (Fig. 1). Indeed, recent structures of Mango I and Mango II aptamers with two variants of the thiazole orange dye (TO1 and TO3) (51) reveal plasticity in the orientation of the dyes in the binding site, with multiple orientations of the benzothiazole and methylquinoline moieties of the dyes as well as multiple orientations of the A-U bases that stack above them (51). In contrast, significant and sigmoidal loss of Hoogsteen basepaired imino proton peak intensities for the G-quadruplex resonances as a function of pressure is only observed at the two lowest salt concentrations, consistent with a volumetric contribution of electrostriction of the potassium ion released upon G-quadruplex disruption under these conditions, in addition to increased hydration and loss of cavities (31). Because G-quadruplex structures are not stable in absence of the central ion, this argues against the pressure-induced population of a native-like, yet dynamic state in which the imino protons are subject to exchange. However, such a native-like state could explain the more limited decrease in imino proton peak intensity with pressure observed at 100 mM KCl.

The different volume change values and salt dependency for the transitions observed by fluorescence and NMR indicate that they report on two separate, but linked

TABLE 2 Thermodynamic Parameters for the NMR-Detected Pressure-Induced Transition in Mango III

		1 mM KCl		10 mM KCl		100 mM KCl	
Peak name	Ω 1 bar	ΔG^o (kcal/mol)	ΔV^o (mL/mol)	ΔG^o (kcal/mol)	ΔV^o (mL/mol)	ΔG^o (kcal/mol)	ΔV^o (mL/mol)
G1 imino	11.27	0 ± 0.5	−57 ± 20	1.6 ± 0.6	−57 ± 8	1.3 ± 0.5	−22 ± 12
G2 imino	11.15	0.3 ± 0.3	−45 ± 20	1.3 ± 0.5	−45 ± 7	2.0 ± 0.5	−30 ± 12
G3 imino	10.93	0.4 ± 0.8	−52 ± 20	2.3 ± 0.7	−52 ± 11	0.1 ± 0.5	−8 ± 12
G4 imino	10.77	0.6 ± 0.6	−61 ± 15	2.3 ± 0.6	−61 ± 10	0.2 ± 0.5	−11 ± 12
Amino	8.6	1.5 ± 0.5	−45 ± 14	1.9 ± 0.5	−45 ± 12	1.4 ± 0.5	−21 ± 12

The signs of ΔG^o and ΔV^o are for the "unfolding" direction of the reaction.

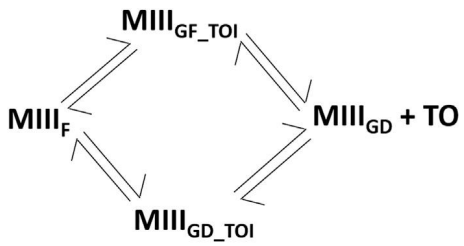

FIGURE 6 Schematic for the transition pathways of Mango III deduced from the high-pressure NMR and fluorescence experiments. MIII$_F$ is fully folded, maximally fluorescent Mango III. MIII$_{GD_TOI}$ is Mango III in which the G-quadruplex is disrupted and the dye is bound in an intermediate fluorescent state. MIII$_{GF_TOI}$ is Mango III in which the G-quadruplex is folded and the dye is bound in an intermediate fluorescent state. Finally, MIII$_{GD}$ + TO is Mango III with disrupted G-quadruplex and free dye.

conformational transitions. At high salt and high pressure, the G-quadruplex of Mango III is minimally perturbed, leading to the population of an intermediate with intermediately fluorescent dye and mostly folded G-quadruplex (MIII$_{GF_TO}$). At lower salt, the G-quadruplex is nearly completely destabilized by pressure, while the dye populates a similarly fluorescent intermediate state (MIII$_{GU_TO}$). If unfolding were to proceed further from this intermediate (which it does not up to 3000 bar pressure), then the dye would dissociate (MIII$_{GU}$ + TO). Transition to this unfolded and dissociated state is highly improbable at high salt, given the stability of the G-qaudruplex. Finally, at higher temperature, the secondary structure of the rest of aptamer would melt (not pictured in Fig. 6). Because, unlike high temperature, high pressure does not strongly affect canonical secondary structures, intermediates such as those revealed here can be more easily populated and characterized.

Implications for in vitro selections

Most aptamers have been discovered in large pools of oligos through affinity-based in vitro selection experiments (i.e., SELEX). Numerous experimental decisions are made when designing such selections to promote desired properties, such as K_d and stability. We observed that Mango III can remain bound to TO even when the quadruplex is not formed. This TO-bound state with disrupted quadruplex may have contributed to the selection of the Mango III sequence over other sequences in the pool. It is not known whether the various conformational states of other Mango structures have this property as well, although as noted, the fluorescence intensity of the states populated under pressure is similar to that observed for Mango IV and higher than that observed for either Mango I and II. It is possible that these three aptamers bind to the TO dye in a similar fashion in solution as the high-pressure intermediates observed here. It would be of interest in the future to compare the affinities of the two bound states for the TO ligand. Our results further highlight the importance of selection protocols in producing molecular properties, even if unintended, and suggest important roles for suboptimal structures during selection experiments.

The importance of pressure in biological systems and origins of life

In addition to the usefulness of high pressure for the analysis of structural conformations, high-pressure environments are abundant on Earth. Numerous extremophiles thrive near deep sea vents, and microbes have been found deep within the continental and oceanic crusts. Both environments can produce pressures of several hundred and even 1000 or more bar. Microbes commonly use RNA structural changes to regulate gene expression (i.e., riboswitches), and it is possible that pressure-induced RNA structural changes might be used for modulating homeostasis in high-pressure organisms. Indeed, the pressure-dependent differential expression of a riboswitch has been reported for the facultative piezophilic *Photobacterium profundum* (56). Future investigations into pressure-induced structural changes of regulatory RNAs from such organisms will provide insight into RNA-dependent biological regulation in these extreme environments.

SUPPORTING MATERIAL

Supporting material can be found online at https://doi.org/10.1016/j.bpj.2021.12.037.

AUTHOR CONTRIBUTIONS

B. Harish prepared the samples, acquired the data, analyzed the data, and wrote the manuscript. J.W. prepared the samples. B.G. and W.H. helped with the 2D NOESY experiments. R.W. and E.H. conceived the study and wrote the manuscript. C.A.R. conceived the study, directed the study, and wrote the manuscript.

ACKNOWLEDGMENTS

This work was supported by National Science Foundation grant CHE 1610691 to CAR, National Aeronautics and Space Administration Grant #80NSSC17K0738, the Human Frontiers in Science Program Grant #RGY077, and the National Science Foundation grants #OIA-1826801 to E.J.B. R.W. acknowledges funding by the Deutsche Forschungsgemeinschaft (DFG, German Research Foundation) under Germany's Excellence Strategy - EXC 2033–390677874 - RESOLV".

REFERENCES

1. Serganov, A., and D. J. Patel. 2007. Ribozymes, riboswitches and beyond: regulation of gene expression without proteins. *Nat. Rev. Genet.* 8:776–790.
2. Woodson, S. A. 2005. Metal ions and RNA folding: a highly charged topic with a dynamic future. *Curr. Opin. Chem. Biol.* 9:104–109.
3. Sengupta, R. N., S. N. S. Van Schie, …, D. Herschlag. 2016. An active site rearrangement within the Tetrahymena group I ribozyme releases

nonproductive interactions and allows formation of catalytic interactions. *RNA.* 22:32–48.

4. Puglisi, J. D., R. Tan, …, J. R. Williamson. 1992. Conformation of the TAR RNA-arginine complex by NMR spectroscopy. *Science.* 257:76–80.
5. Dethoff, E. A., K. Petzold, …, H. M. Al-Hashimi. 2012. Visualizing transient low-populated structures of RNA. *Nature.* 491:724–728.
6. Cruz, J. A., and E. Westhof. 2009. The dynamic landscapes of RNA architecture. *Cell.* 136:604–609.
7. Dethoff, E. A., J. Chugh, …, H. M. Al-Hashimi. 2012. Functional complexity and regulation through RNA dynamics. *Nature.* 482:322–330.
8. Bisaria, N., and D. Herschlag. 2015. Probing the kinetic and thermodynamic consequences of the tetraloop/tetraloop receptor monovalent ion-binding site in P4 – P6 RNA by smFRET. *Biochem. Soc. Trans.* 43:172–178.
9. Bothe, J. R., E. N. Nikolova, …, H. M. Al-Hashimi. 2011. Characterizing RNA dynamics at atomic resolution using solution-state NMR spectroscopy. *Nat. Methods.* 8:919–931.
10. Shi, X., N. Bisaria, …, D. Herschlag. 2014. Roles of long-range tertiary interactions in limiting dynamics of the Tetrahymena group i ribozyme. *J. Am. Chem. Soc.* 136:6643–6648.
11. Russell, R., and D. Herschlag. 2001. Probing the folding landscape of the Tetrahymena ribozyme: commitment to form the native conformation is late in the folding pathway. *J. Mol. Biol.* 308:839–851.
12. Woodson, S. A. 2015. RNA folding retrospective: lessons from ribozymes big and small. *RNA.* 21:502–503.
13. Xue, Y., D. Kellogg, …, H. M. Al-Hashimi. 2015. Characterizing RNA Excited States Using NMR Relaxation Dispersion, First edition. Elsevier Inc.
14. Warner, K. D., M. C. Chen, …, A. R. Ferré-D'Amaré. 2014. Structural basis for activity of highly efficient RNA mimics of green fluorescent protein. *Nat. Struct. Mol. Biol.* 21:658–663.
15. Trachman, R. I., N. Demeshkina, …, A. R. Ferré-D'Amaré. 2017. Structural basis for high-affinity fluorophore binding and activation by RNA Mango. *Nat. Chem. Biol.* 13:807–813.
16. Trachman, R. J. I., A. Autour, …, A. R. Ferré-D'Amaré. 2020. Structure and functional reselection of the Mango-III fluorogenic RNA aptamer. *Nat. Chem. Biol.* 15:472–479.
17. Chen, L., C. M. Roake, …, S. E. Artandi. 2018. An activity switch in human telomerase based on RNA conformation and shaped by TCAB1. *Cell.* 174:218–230.e13.
18. Dumas, L., P. Herviou, …, S. Millevoi. 2020. G-quadruplexes in RNA biology: recent advances and future directions. *Trends Biochem. Sci.* 46:270–283.
19. Vallurupalli, P., G. Bouvignies, and L. E. Kay. 2012. Studying "invisible" excited protein states in slow exchange with a major state conformation. *J. Am. Chem. Soc.* 134:8148–8161.
20. Palmer, A. G. 2004. NMR characterization of the dynamics of biomacromolecules. *Chem. Rev.* 104:3623–3640.
21. Kamatari, Y. O., R. Kitahara, …, K. Akasaka. 2004. High-pressure NMR spectroscopy for characterizing folding intermediates and denatured states of proteins. *Methods.* 34:133–143.
22. Roche, J., C. A. Royer, and C. Roumestand. 2019. Exploring protein conformational landscapes using high-pressure NMR. *Methods Enzymol.* 614:293–320.
23. Akasaka, K. 2006. Probing conformational fluctuation of proteins by pressure perturbation. *Chem. Rev.* 106:1814–1835.
24. Lin, M. C., and R. B. Macgregor. 1997. Activation volume of DNA duplex formation. *Biochemistry.* 36:6539–6544.
25. Macgregor, R. B. 1998. Effect of hydrostatic pressure on nucleic acids abstract. *Biopolymers.* 48:253–263.
26. Rayan, G., A. D. Tsamaloukas, …, H. Heerklotz. 2009. Helix-coil transition of DNA monitored by pressure perturbation calorimetry. *J. Phys. Chem. B.* 113:1738–1742.
27. Dubins, D. N., A. Lee, …, T. V Chalikian. 2001. On the stability of double stranded nucleic acids. *J. Am. Chem. Soc.* 123:9254–9259.
28. Takahashi, S., and N. Sugimoto. 2013. Effect of pressure on the stability of G-quadruplex DNA: thermodynamics under crowding conditions. *Angew. Chem. Int. Ed. Engl.* 52:13774–13778.
29. Takahashi, S., and N. Sugimoto. 2013. Effect of pressure on thermal stability of G-quadruplex DNA and double-stranded DNA structures. *Molecules.* 18:13297–13319.
30. Fan, H. Y., Y. L. Shek, …, T. V. Chalikian. 2011. Volumetric characterization of sodium-induced G-quadruplex formation. *J. Am. Chem. Soc.* 133:4518–4526.
31. Li, Y. Y., D. N. Dubins, …, R. B. Macgregor. 2017. The role of loops and cation on the volume of unfolding of G-quadruplexes related to HTel. *Biophys. Chem.* 231:55–63.
32. Gao, M., B. Harish, …, R. Winter. 2017. Temperature and pressure limits of guanosine monophosphate self-assemblies. *Sci. Rep.* 7:9864.
33. Rayan, G., and R. B. Macgregor. 2015. A look at the effect of sequence complexity on pressure destabilisation of DNA polymers. *Biophys. Chem.* 199:34–38.
34. Macgregor, R., and A. R. Amiri. 2011. Effect of pressure on the stability of short DNA hairpins. *Biophys. J.* 100:356a.
35. Downey, C. D., R. L. Crisman, …, A. Pardi. 2007. Influence of hydrostatic pressure and cosolutes on RNA tertiary structure. *J. Am. Chem. Soc.* 129:9290+.
36. Garcia, A. E., and D. Paschek. 2008. Simulation of the pressure and temperature folding/unfolding equilibrium of a small RNA hairpin. *J. Am. Chem. Soc.* 130:815–817.
37. Ztouti, M., H. Kaddour, …, M.-C. Maurel. 2009. Adenine, a hairpin ribozyme cofactor - high-pressure and competition studies. *FEBS J.* 276:2574–2588.
38. Maurel, M. C., F. Leclerc, and G. Hervé. 2020. Ribozyme chemistry: to be or not to be under high pressure. *Chem. Rev.* 120:4898–4918.
39. Tobé, S., T. Heams, …, S. Tobe. 2005. The catalytic mechanism of hairpin ribozyme studied by hydrostatic pressure. *Nucleic Acids Res.* 33:2557–2564.
40. Hervé, G., S. Tobé, …, M.-C. Maurel. 2006. Hydrostatic and osmotic pressure study of the hairpin ribozyme. *Biochim. Biophys. Acta.* 1764:573–577.
41. Schuabb, C., M. Berghaus, …, R. Winter. 2015. Exploring the free energy and conformational landscape of tRNA at high temperature and pressure. *Chemphyschem.* 16:138–146.
42. Bar-On, Y. M., R. Phillips, and R. Milo. 2018. The biomass distribution on Earth. *Proc. Natl. Acad. Sci. U S A.* 115:6506–6511.
43. Orcutt, B. N., D. E. LaRowe, …, C. G. Wheat. 2013. Microbial activity in the marine deep biosphere: progress and prospects. *Front. Microbiol.* 4:1–15.
44. Colman, D. R., S. Poudel, …, J. R. Spear. 2017. The deep, hot biosphere: twenty-five years of retrospection. *Proc. Natl. Acad. Sci. U S A.* 114:6895–6903.
45. Jebbar, M., B. Franzetti, …, P. Oger. 2015. Microbial diversity and adaptation to high hydrostatic pressure in deep-sea hydrothermal vents prokaryotes. *Extremophiles.* 19:721–740.
46. Orcutt, B. N., J. B. Sylvan, and C. M. Santelli. 2017. Editorial: recent advances in geomicrobiology of the ocean crust. *Front. Microbiol.* 8:1–3.
47. Orsi, W. D., V. P. Edgcomb, …, J. F. Biddle. 2013. Gene expression in the deep biosphere. *Nature.* 499:205–208.
48. Kieft, T. L. 2016. Microbiology of the deep continental biosphere. *In* Their World: A Diversity of Microbial Environments. C. J. Hurst, ed. Springer International Publishing, pp. 225–249.
49. Benner, S. A., E. A. Bell, …, D. Trail. 2019. When did life likely emerge on Earth in an RNA-first process? *ChemSystemsChem.* 2:e1900035.

50. Dolgosheina, A. V., S. C. Y. Jeng, …, P. Unrau. 2014. RNA Mango aptamer-fluorophore: a bright, high affinity, complex for RNA labeling and tracking. *ACS Chem. Biol.* 9:2412–2420.

51. Trachman, R. I., A. Abdolahzadeh, …, A. Ferré-D'Amaré. 2019. Crystal structures of the Mango-II RNA aptamer reveal heterogeneous fluorophore binding and guide engineering of variants with improved selectivity and brightness. *Biochemistry.* 57:3544–3548.

52. Dellarole, M., and C. A. Royer. 2014. High-pressure fluorescence applications. *In* Methods in Molecular Biology. Humana Press, pp. 53–73.

53. Adrian, M., B. Heddi, and A. T. Phan. 2012. NMR spectroscopy of G-quadruplexes. *Methods.* 57:11–24.

54. Knop, J. M., S. Patra, …, R. Winter. 2018. The deep sea osmolyte trimethylamine N-oxide and macromolecular crowders rescue the antiparallel conformation of the human telomeric G-quadruplex from urea and pressure stress. *Chemistry.* 24:14346–14351.

55. Gleitsman, K. R., R. N. Sengupta, and D. Herschlag. 2017. Slow molecular recognition by RNA. *RNA.* 23:1745–1753.

56. Campanaro, S., F. De Pascale, …, G. Valle. 2012. The transcriptional landscape of the deep-sea bacterium Photobacterium profundum in both a toxR mutant and its parental strain. *BMC Genomics.* 13:567–586.